MICROPRESTRESS-SOLIDIFICATION THEORY FOR CONCRETE CREEP. II: ALGORITHM AND VERIFICATION

By Zdeněk P. Bažant,[1] Fellow, ASCE, Anders Boe Hauggaard,[2] and Sandeep Baweja[3]

ABSTRACT: This paper presents a numerical algorithm for the microprestress-solidification theory developed in a companion paper and verifies this theory by comparisons with typical test data from the literature. A model for cracking is incorporated in the algorithm.

INTRODUCTION

The companion paper in this issue (Bažant et al. 1997) presents a generalization of the solidification theory. Compared to the previous solidification theory, the generalization is better justified by the understanding of the physical processes involved in the effects of aging and drying on the creep of concrete. It remains to formulate a numerical algorithm for practical application of this new theory in finite-element programs and to compare the new theory to the main available experimental data. This is the purpose of this paper. All the definitions and notations introduced in the preceding paper are retained.

INCORPORATION OF CRACKING

For concrete exposed to a drying environment, it is necessary to consider distributed cracking. If the specimen or structure is large and drying times long, it is also necessary to consider localization of cracking into continuous cracks and use fracture mechanics, but this situation will not be considered here.

To calculate the strain increments due to cracking, the crack band theory is used (Bažant and Oh 1983). The cracking strain is assumed to be additive to creep and shrinkage strains [Fig. 1(c)]. We are concerned only with cylinders subjected to symmetrical loading and, therefore, only cracking in the three orthogonal orientations normal to axes r, θ, and z [Fig. 1(a)] is considered. Cracking is initiated when the stress reaches the tensile strength (f'_t). After that, a linear softening stress-crack strain diagram of slope C_f, as shown in Fig. 1(b) is followed ($C_f < 0$). The material parameters needed to define this are the tensile strength (f'_t) and the strain at zero stresses (ε_0). Unloading in Fig. 1(b) follows a vertical slope, which implies that the unloading slope for the material as a whole [Fig. 1(d)] is the elastic modulus E. The area under the stress-strain diagrams in Fig. 1(b and c) must be equal to G_f/h where G_f = fracture energy of the material and h = crack band width. The slope of the descending branch shown in Fig. 1(c) is given by $E_t = (C_f^{-1} - E^{-1})^{-1}$.

The rate of cracking strains for the axisymmetric case may be written as $\dot{\varepsilon} = \mathbf{C}_s\dot{\sigma}$, where the crack compliance matrix is given by (Bažant and Oh 1983)

$$\mathbf{C}_s = \begin{bmatrix} C_f^{-1} & 0 & 0 & 0 \\ 0 & C_f^{-1} & 0 & 0 \\ 0 & 0 & C_f^{-1} & 0 \\ 0 & 0 & 0 & 0 \end{bmatrix} \qquad (1)$$

However, since the role of cracking on the planes normal to the radial coordinate r is negligible, the first diagonal term of the matrix was replaced in computations by 0.

Without cracking it would be impossible to model the large strain difference between the creep specimen and its companion shrinkage specimen that appears initially after the start of drying. This strain difference is illustrated in Fig. 2, which also shows the microprestress flow term for drying environments at 50 and 75% relative humidity (RH).

It must be emphasized that the concept of smeared cracking must be replaced by fracture mechanics if the cracking can localize into continuous cracks. According to Bažant and Raftshol (1982), this is probably unimportant for normal size laboratory specimens, but is important for more massive specimens and larger structural members [see also Planas and Elices (1993)].

APPLICATION OF EXPONENTIAL ALGORITHM FOR TIME STEPS

Time is subdivided by discrete times t, ($i = 1, 2, \ldots$) into time steps $\Delta t = t_{i+1} - t_i$. The quantities corresponding to time t_i are labeled by subscript i. The distributions of pore humidity h and microprestress S are solved first, in advance of structural analysis. The solution of h is reviewed in Appendix I.

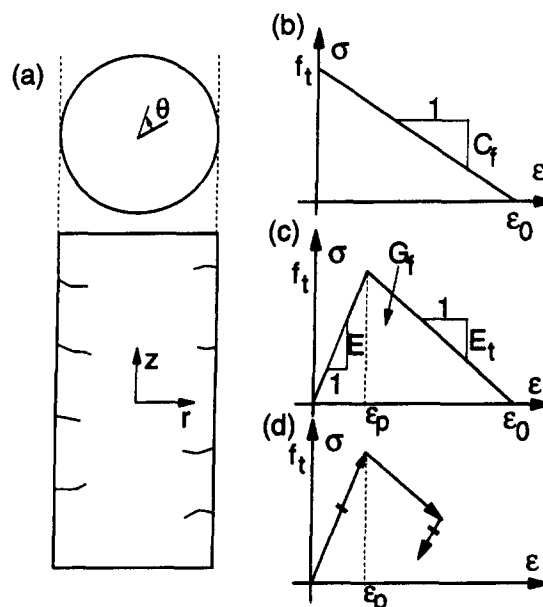The solution of S is obtained step-by-step by integrating the

FIG. 1. (a) Crack Orientations Considered; (b) Relation of Normal Stress to Cracking Strain with Postpeak Strain Softening; (c) Rule Assumed for Unloading of Cracks; (d)
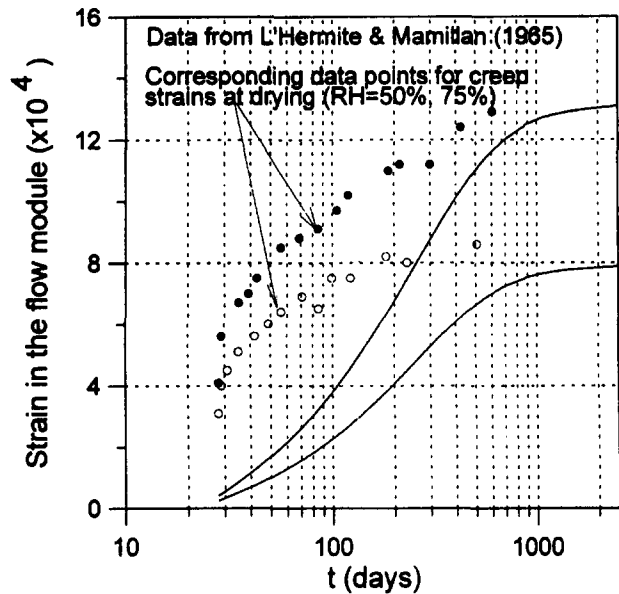
FIG. 2. Microprestress Flow Term without Effect of Cracking

first-order differential equation (6) of Part I of the companion paper. For the step (t_i, t_{i+1}), one obtains

$$S_{i+1} = S_i - c_0 S_{i+1/2}^p \Delta t - c_1 \frac{\Delta h}{h_{i+1/2}} \quad (2)$$

where Δh and ΔS = increments over Δt and the value of $S_{i+1/2}$ is taken as S_i for the first iteration and $S_i + \Delta S/2$ for the second iteration of step (t_i, t_{i+1}) (this is actually the Runge-Kutta algorithm).

For the special case that $p = 2$ as considered here, it is more accurate and preferable to integrate Eq. (6) of the companion paper exactly [e.g., Rektorys (1994), Sec. 17.2] under the simplifying assumption that $d \ln h/dt$ is constant within each time step and changes only by jumps between the steps. In that case

$$S_{i+1} = \frac{S_i - c_1 \omega \Delta(\ln h)}{1 + c_0 S_i \omega \Delta t} \quad (3)$$

where

$$\omega = (\tan \Delta\xi)/\Delta\xi \quad \text{for} \quad \Delta h > 0 \text{ and } \Delta\xi > 10^{-5} \quad (4)$$

$$\omega = (\tanh \Delta\xi)/\Delta\xi \quad \text{for} \quad \Delta h < 0 \text{ and } \Delta\xi > 10^{-5} \quad (5)$$

$$\omega = 1 \quad \text{for} \quad \Delta\xi \leq 10^{-5} \quad (6)$$

and

$$\Delta\xi = \sqrt{c_0 c_1 \Delta t |\Delta \ln h|} \quad (7)$$

The last formula is exact only for $\Delta h = 0$. It is introduced for $|\Delta h| \leq 10^{-4}$ because the numerical accuracy in evaluating the two preceding formulas breaks down as $\Delta h \rightarrow 0$.

For uniaxial stress, an efficient, unconditionally stable step-by-step solution algorithm, which was of the exponential algorithm type [Bažant (1971); Bažant and Chern (1985); Bažant (1988), Chap. 2], was given by (5–14) in Bažant and Prasannan (1989b). In an algorithm of this type, the differential equations of the constitutive law are integrated for each time step exactly under the simplifying assumption that the strain rate and all the age-dependent coefficients are constant within the time step and change only by jumps between the steps. In view of (15) in the companion paper, this algorithm may be generalized to multiaxial stress by replacing σ with $G\sigma$, ε with ε, etc. The matrix generalization of the recursive

relation for γ_μ [Eq. 5 in Bažant and Prasannan (1989b)] yields the following exponential algorithm formulas:

$$\gamma_{\mu_{i+1}} = \kappa_\mu \gamma_{\mu_i} + \frac{1 - \kappa_\mu}{E_\mu} G\sigma + \frac{1 - \lambda_\mu}{E_\mu} G\Delta\sigma \quad (8)$$

where

$$\kappa_\mu = e^{-\Delta y_\mu}, \quad \lambda_\mu = \frac{1 - \kappa_\mu}{\Delta y_\mu} \quad \text{and} \quad \Delta y_\mu = \frac{\Delta t}{\tau_\mu} \quad (9)$$

Note that $0 \leq \lambda_\mu \leq 1$. For $\Delta t \ll \tau_\mu$, λ_μ approaches 1, which means that the response of the Kelvin unit is almost the same as the response of the dashpot alone, with the effect of the spring being negligible. For $\Delta t \gg \tau_\mu$, λ_μ approaches 0, which means the Kelvin unit μ responds almost the same as a spring, with the effect of dashpot being negligible. This feature makes the exponential algorithm numerically stable for arbitrarily large Δt. Evaluating $\Delta\gamma = \Sigma_\mu (\gamma_{\mu_{i+1}} - \gamma_{\mu_i})$, we obtain

$$\Delta\gamma = C_N G\Delta\sigma + \Delta\gamma'' \quad (10)$$

where

$$C_N = \sum_{\mu=1}^{N} \frac{1 - \lambda_\mu}{E_\mu} \quad (11)$$

and

$$\Delta\gamma'' = \sum_{\mu=1}^{N} (1 - \kappa_\mu) \left(\frac{1}{E_\mu} G\sigma_i - \gamma_{\mu_i} \right) \quad (12)$$

Applying the central difference approximation over Δt to the matrix Eq. (18) of Part I of the companion paper provides

$$\Delta\varepsilon^v = \begin{bmatrix} \phi_h \\ v \end{bmatrix}_{i+1/2} \quad \text{and} \quad \Delta\gamma = \begin{bmatrix} \phi_h \\ v \end{bmatrix}_{i+1/2} (C_N G\Delta\sigma + \Delta\gamma'') \quad (13)$$

where subscript $i + 1/2$ refers to the average value in the time step. Finally, adding [as shown in Fig. 1(c) in the companion paper] the matrix generalization of the viscous flow strain $(\Delta\varepsilon^f)$ of the instantaneous elastic strain $(q_1 G\Delta\sigma)$, of the shrinkage strain (Δe_{sh}) and of the cracking strain $\Delta\varepsilon_{cr} = C_r \Delta\sigma$, we obtain the incremental quasielastic stress-strain relations
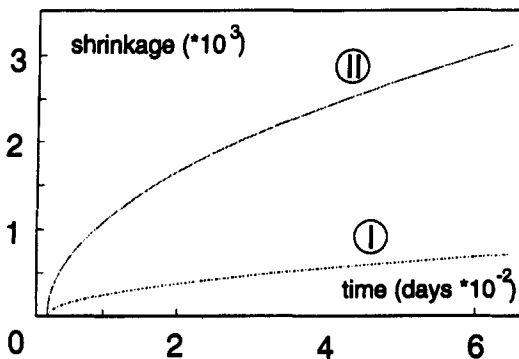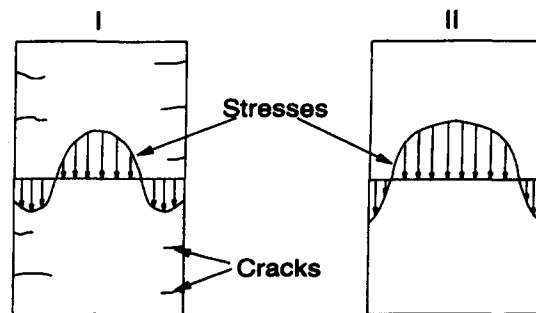

FIG. 3. Stresses and Shrinkage in Cracked and Uncracked Specimen (I) (II)

$$\Delta\sigma = E(\Delta\varepsilon - \Delta\varepsilon'') \tag{14}$$

where E = incremental stiffness matrix given by

$$E = \left[G^{-1} \left(q_1 + A_0 \left[\frac{\phi_h}{v} \right]_{i+1/2} + C_N \left[\frac{\phi_h}{v} \right]_{i+1/2} \right) + C_s \right]^{-1} \tag{15}$$

and where $\Delta\varepsilon''$ = incremental inelastic strains given by

$$\Delta\varepsilon'' = \left[\frac{\phi_h}{v} \right]_{i+1/2} \Delta\gamma'' + \frac{\Delta t}{\eta_{i+1/2}} G\sigma_{i+1/2} + \Delta\varepsilon_{sh} \tag{16}$$

where E = incremental quasielastic stiffness matrix of the material; and $\Delta\varepsilon''$ = total inelastic strain increment during Δt.

The following algorithm of finite-element analysis may be used in each time step (t_i, t_{i+1}), in which the values of σ_i, ε_i, ε_i^v, ε_i^f, γ_i, and γ_{μ_i} for the beginning of the time step are already known form the solution of the preceding step.

1. Estimate $\sigma_{i+1/2} = \sigma_i + \Delta\sigma/2$ for all integration points (of all finite elements) using for $\Delta\sigma$ the value obtained in the preceding iteration of the step, or for the first iteration, the value obtained in the previous loading step. Then, using (10), (11), (12), (15), and (16), calculate C_N, $\Delta\gamma''$, $\Delta\gamma$, E, and $\Delta\varepsilon''$ for all the integration points.
2. Solve the structure using the quasielastic stress-strain relation (14) along with the load and displacements increments prescribed for this time step. Check the chosen tolerance for the termination of iterations and if it is not

met, return to Step 1 and start the next iteration of this time step. Otherwise evaluate $\sigma_{i+1} = \sigma_i + \Delta\sigma$, $\gamma_{i+1} = \varepsilon_i + \Delta\varepsilon$, $\gamma_{\mu_{i+1}} = \gamma_{\mu_i} + \Delta\gamma_\mu$, etc. for all the points of the structure, return to Step 1 and start the first iteration of the next step.

COMPARISON TO AVAILABLE EXPERIMENTAL EVIDENCE

In creep measurements in drying environment, it is standard not to report the total deformation but report separately the drying shrinkage strain of load-free companion specimen and the compliance representing the difference in strain per unit stress between the loaded creep specimen and the load-free companion specimen. The creep value thus defined, however, is affected by microcracking of the companion shrinkage specimen, which relieves the tensile stresses due to drying and strongly reduces the overall shrinkage deformations (Fig. 3).
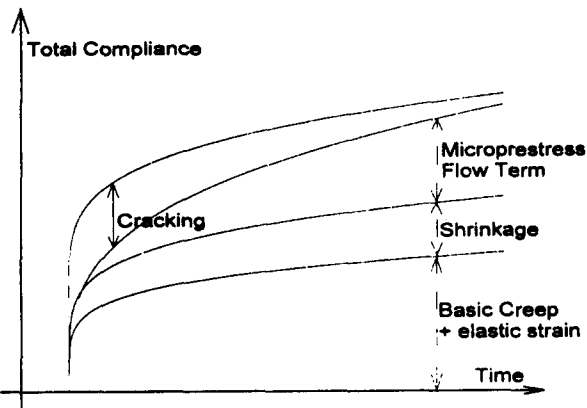
FIG. 4. Contributions from Various Mechanisms of Drying Creep
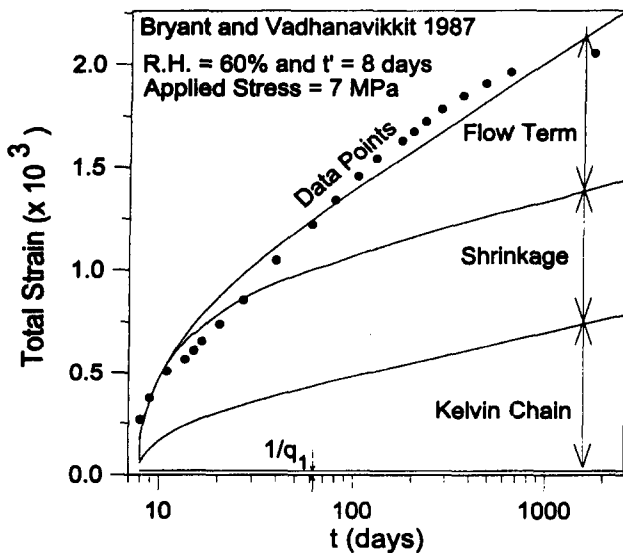
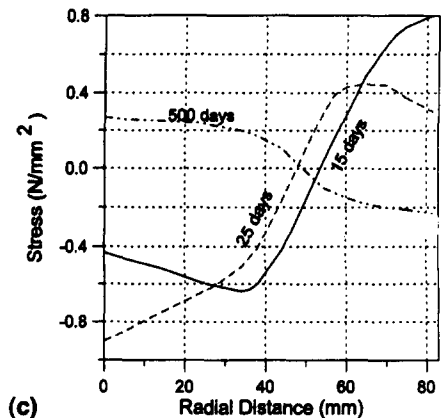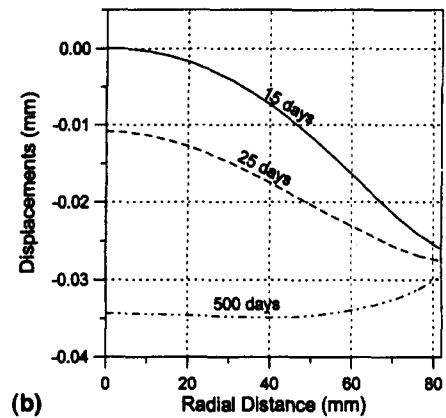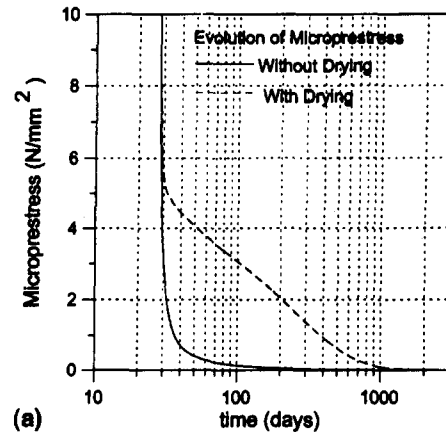FIG. 5. Separation of Strains for Test Data of Bryant and Vadhanavikkit (1987), $t' = 8$ d

FIG. 6. (a) Evolution of Microprestresses with and without Drying; (b) Displacements in Drying Specimen; (c) Stresses in Drying Specimen

Thus, when the deformations measured on the companion specimen [(I) in Fig. 3] are subtracted from the deformations measured on the loaded and drying specimen, it is not only the true creep that remains but also the cracking deformations of the companion specimen (Fig. 4). This explains why some reported drying creep measurements show a large strain increase immediately after loading, compared to the nondrying loaded specimen [e.g., L'Hermite et al. (1965)]. Cracking, albeit milder, appears even in the creep specimen that is subjected to compressive load [e.g., Granger et al. (1994)], and therefore it is not easy to separate cracking in the companion drying specimen from cracking in the loaded drying specimen.

When a three dimensional analysis of the drying loaded specimens is performed, it is essential to know the locations of measurement points on the specimen, i.e., the precise points the displacements of which were measured and used to determine the strains reported. The reason is that, at the specimen surface, a drying environment gives large shrinkage strains immediately after exposure whereas a long time is required for the drying to reach the core. Many reports on test data in the literature do not indicate the locations of the measurement points and, therefore, are not very useful for the present purpose.

VERIFICATION AND CALIBRATION BY TEST DATA

Bryant and Vadhanavikkit's (1987) Data

Square prisms of sides a = 150 mm and length l = 600 mm were exposed to a drying environment of RH 60%. After 8 days of curing, relative displacements were measured on the specimen surface. The axial compressive stress was -7 MPa. To enable axisymmetric analysis of moisture diffusion and deformation that simplifies programming, it is assumed that the strains are the same as in an equivalent cylinder of volume-to-surface ratio $(V/S)_c = (V/S)_p c_p/c_c$ where $(V/S)_p = a/4$ = volume-to-surface ratio of prism and c_c = 1.15, and c_p = 1.25 are the shape correction coefficients based on the results of the study of Bažant et al. (1976). The basic creep strains and strains at drying for three different ages at loading (t' = 8, 28,
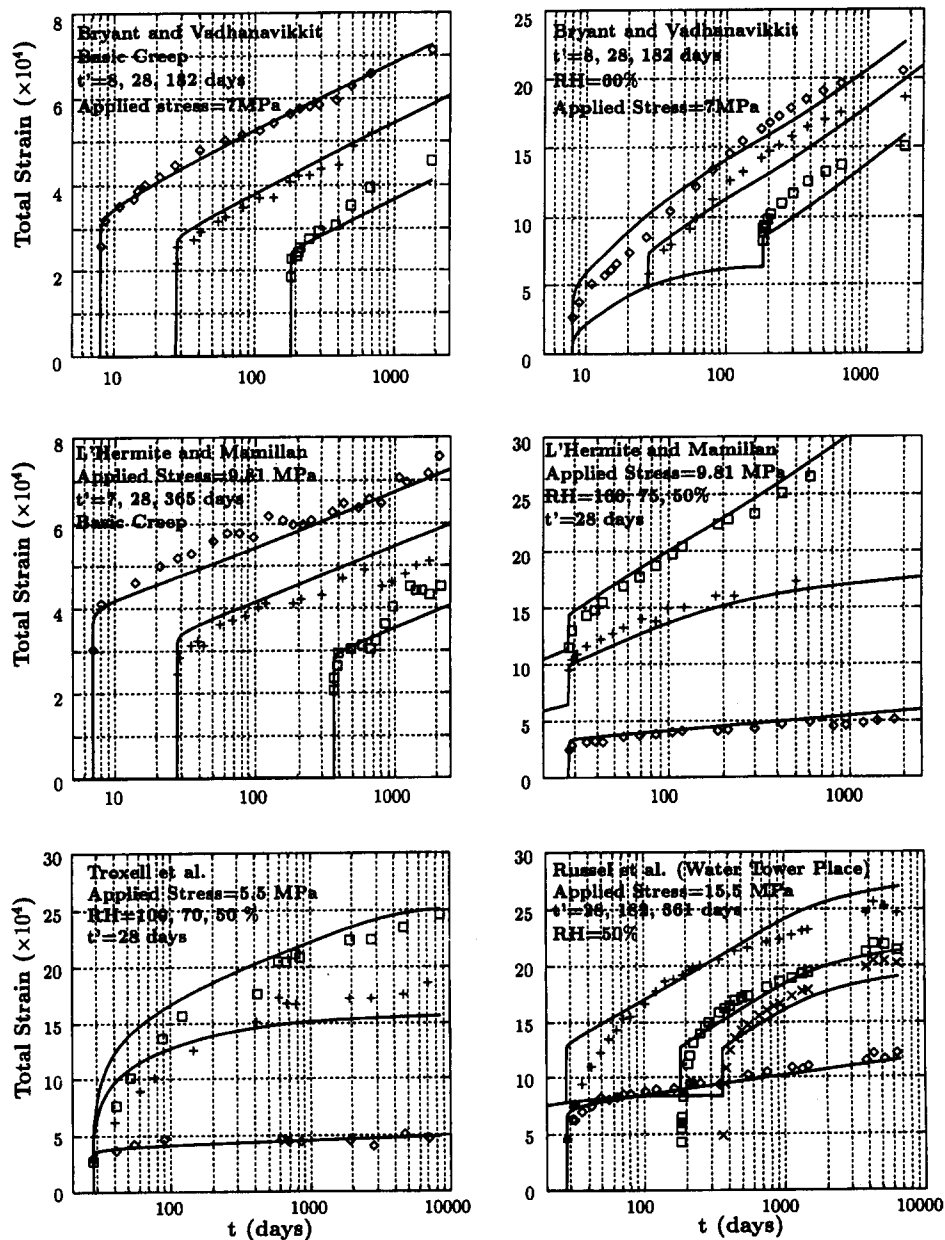

FIG. 7. Fit of Basic Creep and Total Strains at Drying by L'Hermite et al. (1965); Troxell et al. (1958); Russell and Corley (1977); Bryant and Vadhanavikkit (1987)

TABLE 1. Values of Coefficients Used in Comparison with Test Data

Tests (1)	$S_0^2 = 25.26$; $S_0^{182} = 1.01$[a] (2)	$S_0^7 = 5.5$; $S_0^{365} = 0.32$[b] (3)	[c] (4)	$S_0^{182} = 0.143$; $S_0^{361} = 2.7 \times 10^{-3d}$ (5)
q_1 (MPa⁻¹)	2.03×10^{-5}	2.4×10^{-5}	2.7×10^{-5}	1.48×10^{-5}
q_2 (MPa⁻¹)	3.9×10^{-5}	5.3×10^{-5}	5.3×10^{-5}	6.1×10^{-4}
α	1.4×10^{-2}	8.5×10^{-3}	4.2×10^{-3}	1.9×10^{-2}
α_h	0.5	0.5	0.75	0.65
c (1/[(MPa)² s])	1.59×10^{-6}	2.72×10^{-6}	3.44×10^{-6}	1.03×10^{-5}
c_0 (1/[(MPa) s])	0.49	0.94	1.79	1.35
c_1 (MPa)	1.98	8.2	13.2	22.4
S_0^{28} (MPa)	2.89	1.7	19.4	0.143
k_{sh}	1.83×10^{-3}	2.62×10^{-3}	4.73×10^{-3}	5.7×10^{-3}
E (MPa)	4.92×10^{4}	3.85×10^{4}	5.27×10^{4}	8.31×10^{4}
f_c' (MPa)	1.8	1.4	1.2	2.4
ε_0	2.53×10^{-4}	1.68×10^{-4}	4.74×10^{-4}	9.23×10^{-4}
D (mm/day)	0.84	1.35	0.25	4.32
C (mm²/day)	35.3	24.9	36.3	45.8

Note: Test values in molar pascals.
[a]Bryant and Vadhanavikkit (1987).
[b]L'Hermite et al. (1965).
[c]Troxell et al. (1958).
[d]Russell and Corley (1977).

and 182 days) are analyzed. Fig. 5 shows the different terms contributing the strains fitted for the drying specimen with t' = 8 days. Fig 6(a) shows how the microprestress, with and without drying, develops in time. To illustrate the behavior of the load-free drying specimen, Fig. 6(b) shows the deformations as a function of time. Fig. 6(c) shows the corresponding stress profiles, from which one can see how cracking influences the stresses. The optimum fits achieved are shown in Fig. 7 for basic creep strain and the total strain of loaded specimen at drying (the sum of shrinkage, elastic, and creep strains). Table 1 gives the material parameters corresponding to the fits of these data as well as the data to be considered next. The exponent of the power law for microprestress was taken as $p = 2$.

L'Hermite et al.'s (1965) Data

The tests of basic creep included three different ages at loading (t' = 7, 28, and 365 days) and those of drying creep included one age at loading (t' = 28 days) and three different environmental RH (100, 75, and 50%) with exposure beginning at $t_0 = 1$ day. The specimens were square prisms of $a = 70$ mm and $l = 280$ mm. The measurements were taken on the surface. The axial compression stress was -9.81 MPa. The results are shown in Fig. 7 for the basic creep strains and for the total drying strains. The data points for basic creep reported for t' = 28 and 365 days and ages larger than 800 days are excluded from the present comparison because it is likely that some uncontrollable disturbances occurred because the scatter is very large and decrease of creep with time takes place, which is physically impossible.

Troxell et al.'s (1958) Data

These tests included one age at loading (t' = 28 days) and three different environmental RH (100, 70, and 50%) with exposure starting at $t_0 = 28$ days. The specimens were cylinders of diameter 102 mm and length 365 mm, and the measurements were taken on the surface. The axial compressive stress was -5.5 MPa. Fig. 7 shows the results.

Russell and Corley's (1987) Data

These included one age at loading for basic creep (t' = 28 days) and three ages at loading for tests at drying (t' = 28, 182, and 361 days). Exposure to environment of RH = 50%

started at $t_0 = 7$ days. The specimens were cylinders of diameter 152 mm and length 305 mm. The measurements were taken on the surface and the axial compressive stress was -15.5 MPa. Fig. 7 shows the results.

Previously it was speculated that the discrepancy between the strong long-term age effect on creep and the absence of long-term volume growth of hydration products could be explained by polymerization of calcium silicate hydrates, i.e., formation of new bonds that stiffens the microstructure. However, this speculation has not been justified in detail and, in view of the present theory, may be abandoned.

CONCLUSIONS

1. In the previously formulated solidification theory for basic creep of concrete, aging is explained by the volume growth of a nonaging viscoelastic material (the cement gel) into the pores. Although this theory agrees with the available test data as well as one might hope in view of inevitable random scatter, it has, from the physical viewpoint, the following two shortcomings: (1) The effect of age at loading on the creep compliance remains strong even after many years, whereas the volume growth of the hydration products ceases after about 1 year; and (2) the drying creep (Pickett effect) is not explained by the theory and its modeling requires separate assumptions. The present improvement of solidification theory removes these shortcomings and brings about simplification and unification.

2. The long-term aging, which cannot be accounted for by the volume growth of hydration products, can be explained by relaxation of a tensile microprestress in the bonds or bridges across the micropores in hardened cement gel filled by hindered adsorbed water. The microprestress represents a reaction to the disjoining pressure exerted on the micropore walls by hindered adsorbed water and its initial buildup is caused by high local shrinkage and crystal growth pressure at locations close to the micropore.

3. The long-term creep, deviatoric as well as volumetric, is considered to originate from viscous shear slips between the opposite walls of the micropores in which the bonds or bridges that cross the micropores (and carry the microprestress) break and form again in a manner similar to the movement of dislocations through a crystal lattice. The shear has the property that bonds can restore, and thus the macroscopic stiffness of concrete does not get reduced (tensile breaks do not allow bond restorations; rather they lead to cracks and reduced macroscopic stiffness, which characterizes the nonlinear creep above the service stress range).

4. Due to creep in the direction transverse to the slip plane, the tensile microprestress undergoes relaxation. This relaxation reduces the effective viscosity of the shear slips and thus brings about long-term aging associated with the flow term in the creep model.

5. Because the tensile microprestress S is the reaction to the disjoining pressure, it changes with the disjoining pressure, which in turn changes almost instantaneously with the relative humidity h in the adjacent capillary pore in the hardened cement paste. In consequence, S depends linearly on h. This is the cause of the Pickett effect (drying creep or stress-induced shrinkage).

6. Analysis of the available test data confirms that the microprestress relaxation needs to be introduced only for the viscous flow term of the solidification theory. The dashpots in the Kelvin units of the chain need not be considered affected by any microprestress. Their viscosity varies only as a consequence of volume growth. On

the other hand, the volume growth does not affect the flow term. This separation of the effects of volume growth and microprestress greatly simplifies the mathematical formulation.

7. Good agreement with the available test results, as good as that of the previous solidification theory, can be achieved with the present model, which is simpler. Cracking must, of course, be taken into account in simulating the tests, and the diffusion problem of drying must be solved.

8. The existing form of the solidification theory for basic creep of concrete (Bažant and Prasannan 1989a) as well as Model B3 based on it (Bažant and Baweja 1995) does not need to be changed as a result of the present analysis. What needs to be changed for basic creep (i.e., creep at constant water content) is only the interpretation—the viscous flow term of the original solidification theory expression for the compliance function is not due to volume growth of hydration products into the pores, but is due to relaxation of tensile microprestress. For drying creep, the results of the present theory are different, but not significantly different, from those of the previous combination of solidification theory with stress-induced shrinkage (Bažant and Chern 1985, 1987; Bažant and Xi 1995). This is not surprising, because the present formulation can be regarded as a refinement of these previous formulations.

ACKNOWLEDGMENTS

APPENDIX I. PORE HUMIDITY SOLUTION AND FINITE ELEMENT ANALYSIS

The humidity profiles are obtained by solving the nonlinear diffusion problem governed by the field equations (e.g. Bažant 1988)

$$\dot{h} = -k \text{ div } \mathbf{J} + \dot{h}_s, \qquad \mathbf{J} = -\lambda \text{ grad } h \qquad (17)$$

where $\mathbf{J}$ = moisture flux; λ = moisture permeability of concrete; k = inverse slope of desorption isotherm of concrete; and $\dot{h}_s$ = rate of selfdessication, which was neglected. For the sake of simplicity, k was assumed constant. Then the moisture diffusivity is $D = k\lambda$. It was shown (Bažant and Najjar 1972) to depend on h approximately as

$$D(h) = D_1 \left(\alpha_0 + \frac{1 - \alpha_0}{1 + \left(\dfrac{1 - h}{1 - h_c} \right)^n} \right) \qquad (18)$$

where $\alpha_0 = 0.05$; $n = 6$; $h_c = 0.75$; and D_1 represents the diffusivity at saturation ($h = 1$). At unsealed surface, h was assumed to be equal to RH of environment. As reviewed in Bažant and Thonguthai (1979) and Bažant and Kaplan (1996), the two-dimensional finite-element formulation was obtained applying Galerkin weighting procedure to (17) and then introducing the approximations

$$h = \mathbf{N}\mathbf{h}_n \qquad \nabla h = \mathbf{B}\mathbf{h}_n \qquad \text{and} \quad \dot{h} = \mathbf{N}\dot{\mathbf{h}}_n \qquad (19)$$
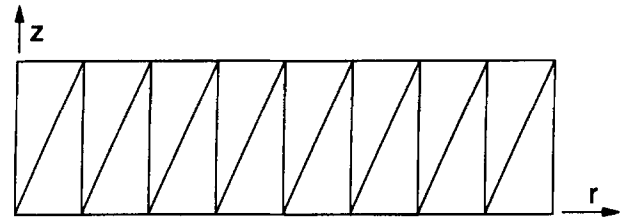
FIG. 8. Finite-Element Mesh Used to Analyze Cylindrical Test Specimens

where $\mathbf{N}$ = humidity interpolation matrix; and $\mathbf{B}$ = humidity gradient interpolation matrix. Then the finite-element equations are

$$\mathbf{C}\dot{\mathbf{h}} + \mathbf{K}\mathbf{h} = \mathbf{R} \qquad (20)$$

where $\mathbf{K}$ = moisture diffusivity matrix; $\mathbf{C}$ = capacity matrix; and $\mathbf{R}$ = moisture load vector. A detailed description of the solution method was given by Hauggaard et al. (1996).

In axisymmetric finite-element analysis of structural response, the generalized displacements are $\mathbf{u} = (u_r, u_z)^T$, and the generalized strains and stresses are $\boldsymbol{\varepsilon} = (\varepsilon_r, \varepsilon_\phi, \varepsilon_z, \gamma_{rz})^T$ and $\boldsymbol{\sigma} = (\sigma_r, \sigma_\theta, \sigma_z, \tau_{rz})^T$. The incremental formulation of the principle of virtual work is [e.g., Damkilde (1983)]

$$\int_V \Delta\boldsymbol{\sigma}^T \delta\boldsymbol{\varepsilon} \, dV = \int_V \mathbf{f}^T \delta\mathbf{u} \, dV + \int_A \mathbf{p}^T \delta\mathbf{u} \, dA - \int_V \boldsymbol{\sigma}_i^T \delta\boldsymbol{\varepsilon} \, dA \qquad (21)$$

where V and A are the volume and surface of structure, respectively; $\mathbf{f}$, $\mathbf{p}$ = given distributed volume and surface load; $\boldsymbol{\sigma}_i$ = stresses at the beginning of the increment; and $\Delta\boldsymbol{\sigma}$ = stress increment. Insertion of the constitutive equation (14) gives

$$\int_V \Delta\boldsymbol{\varepsilon}^T \mathbf{E} \delta\boldsymbol{\varepsilon} \, dV - \int_V \Delta\boldsymbol{\varepsilon}''^T \mathbf{E} \delta\boldsymbol{\varepsilon} \, dV = \int_V \mathbf{f}^T \delta\mathbf{u} \, dV$$
$$+ \int_A \mathbf{p}^T \delta\mathbf{u} \, dA - \int_V \boldsymbol{\sigma}_i^T \delta\boldsymbol{\varepsilon} \, dA \qquad (22)$$

and insertion of the finite-element approximation $\mathbf{u} = \mathbf{N}\mathbf{v}$ and $\Delta\boldsymbol{\varepsilon} = \mathbf{B}\Delta\mathbf{V}$ gives

$$\mathbf{K}_T \Delta\mathbf{V} = \mathbf{R} - \mathbf{R}_i \qquad (23)$$

where $\mathbf{K}_T = \int_V \mathbf{B}^T \mathbf{E} \mathbf{B} \, dV$ is the structural stiffness matrix; $\mathbf{R} = \int_V \mathbf{B}^T \mathbf{E} \Delta\boldsymbol{\varepsilon}'' \, dV + \int_V \mathbf{N}^T \mathbf{f} \, dV + \int_A \mathbf{N}^T \mathbf{p} \, dA$ is the load vector; and $\mathbf{R}_i = \int_V \mathbf{B}^T \boldsymbol{\sigma}_i \, dA$ is the internal load vector corresponding to the stress state. Fig. 8 shows the finite-element mesh; 16 linear-strain triangles were used throughout the diameter of the cylindrical specimens. The solution was done in time steps, iterating the solution of the equation system within each step.

APPENDIX II. REFERENCES

Bažant, Z. P. (1971). "Numerically stable algorithm with increasing time steps for integral-type aging creep." *Proc., 1st Int. Conf. on Struct. Mech. in Reactor Tech. (SMiRT-1)*, Commission of European Communities, Brussels, Belgium. T. A. Jaeger, ed., 119–126.

Bažant, Z. P., and Baweja, S. (1995). "Creep and shrinkage prediction model for analysis and design of concrete structures—Model B3." *Mat. and Struct.*, Paris, France, 28, 357–365. 415–430.

Bažant, Z. P., and Chern, J.-C. (1985a). "Concrete creep at variable humidity: constitutive law and mechanism." *Mat. and Struct.*, Paris, France, 18(103), 1–20.

Bažant, Z. P., and Chern, J.-C. (1985b). "Strain-softening with creep and exponential algorithm." *J. Engrg. Mech.*, ASCE, 111(3), 391–415.

Bažant, Z. P., and Chern, J.-C. (1987). "Stress-induced thermal and shrinkage strains in concrete." *J. Engrg. Mech.*, ASCE, 113(10), 1493–1511.

Bažant, Z. P., Hauggaard, A. B., Baweja, S., and Ulm, F.-J. (1997).

"Microprestress-solidification theory for concrete creep. I: Aging and drying effects." *J. Engrg. Mech.*, ASCE 123(11), 1188–1194.

Bažant, Z. P., and Oh, B. H. (1983). "Crack band theory for fracture of concrete." *Mat. and Struct.*, Paris, France, 16(93), 155–177.

Bažant, Z. P., and Prasannan, S. (1989a). "Solidification theory for concrete creep. I: Formulation." *J. Engrg. Mech.*, ASCE, 115(8), 1691–1703.

Bažant, Z. P., and Prasannan, S. (1989b). "Solidification theory for concrete creep. II: Verification and application." *J. Engrg Mech.*, ASCE, 115(8), 1704–1725.

Bažant, Z. P., and Raftshol, W. J. (1982a). "Effect of cracking in drying and shrinkage specimens." *Cement and Concrete Res.*, 12, 209–226.

Bažant, Z. P., and Raftshol, W. J. (1982b). "Discussion of 'Effect of cracking in drying and shrinkage specimens.'" *Cement and Concrete Res.*, 12, 797–798.

Bažant, Z. P., and Xi, Y. (1995). "Continuous retardation spectrum for solidification theory of concrete creep." *J. Engrg. Mech.*, 121(2), 281–288.

Bryant, A. H., and Vadhanavikkit, C. (1987). "Creep, shrinkage-size, and age at loading effects." *ACI Mat. J.*, 117–123.

Granger, L., Acker, P., and Torrenti, J.-M. (1994). "Discussion of 'Drying creep of concrete: constitutive model and new experiments separating its mechanisms.'" *Mat. and Struct.*, Paris, France, 27, 616–619.

L'Hermite, R., Mamillan, M., and Lefèvre, C. (1965). "Nouveaux résultats de recherches sur la déformation et la rupture du béton." Supplément aux annales de l'institut technique du bâtiment et des travaux publics, 207/208, 325–345 (in French).

Planas, J., and Elices, M. (1993). "Drying shrinkage effect on the modulus of rupture." *Proc., 5th Int. RILEM Symp. on Creep and Shrinkage of Conc. (ConCreep 5)*, Z. P. Bažant and I. Carol, eds., E & FN Spon, London, U.K., 357–368.

Rektorys, K. (1994). *Survey of applicable mathematics.* Kluwer Academic Publishers, Dordrecht-Boston, Mass.

Russell, H. G., and Corley, W. G. (1977). "Time-dependent behavior of columns in water tower place." *Bull. RD052.01B*, Portland Cement Assn. Res. and Develop., Portland, Oreg.

Troxell, G. E., Raphael, J. M., and Davis, R. E. (1958). "Long-time creep and shrinkage tests of plain and reinforced concrete," *ASTM Proc.*, 58, 1101–1120.